Available online at www.sciencedirect.com
SCIENCE DIRECT®
Journal of Molecular Catalysis A: Chemical 226 (2005) 93–100
JOURNAL OF MOLECULAR CATALYSIS A: CHEMICAL
www.elsevier.com/locate/molcata

Preparation of an active SO_4^{2-}/TiO_2 photocatalyst for phenol degradation under supercritical conditions

Hexing Li*, Guisheng Li, Jian Zhu, Ying Wan

Department of Chemistry, Shanghai Normal University, Shanghai 200234, P.R. China

Received 13 May 2004; received in revised form 9 September 2004; accepted 13 September 2004
Available online 5 November 2004

Abstract

SO_4^{2-}-doped TiO_2 (SO_4^{2-}/TiO_2) nanoparticles (SO_4^{2-}/TiO_2) were prepared by the sol–gel method followed by drying the precursor in supercritical ethanol fluid. During the liquid-phase phenol photocatalytic degradation, the as-prepared SO_4^{2-}/TiO_2 exhibited higher activity and longer lifetime than either the undoped TiO_2 or the SO_4^{2-}/TiO_2 obtained through direct drying, apparently as a result of the superiority of the supercritical drying and the promotion of the SO_4^{2-}-dopant. Based on various characterizations including XRD, TEM, XPS, FTIR, and photoluminescence spectra, and FTIR-pyridine thermodesorption, the crystallization degree, the surface area, the pore structure, the surface acidity and the surface electronic state of the as-prepared SO_4^{2-}/TiO_2 samples were investigated and their correlation to the catalytic properties was discussed.

Keywords: Supercritical drying; TiO_2 nanoparticles; SO_4^{2-}-dopant; Photocatalysis; Phenol degradation

1. Introduction

Photocatalysis has been widely used in complete mineralization of organic pollutants in wastewater and air [1–4]. Among various photocatalysts, TiO_2 is most frequently employed owing to its cheapness, nontoxicity, and structural stability [5–10]. However, TiO_2 could be activated only by UV light due to its high-energy band gap (ca. 3.2 eV for anatase). Besides, the low quantum efficiency of the TiO_2 also seems a problem limiting its application. Up to now, nearly all the TiO_2 photocatalysts are prepared by the sol–gel method followed by direct drying and calcinaion to remove the organic compounds and the solvent in the wet gel [11,12]. Although, great attempts have been made to improve the catalytic performance of the TiO_2 photocatalyst, such as modification with metallic ions or other oxides [13], very little attention has been paid to development of new preparation methods. As well known, the quantum efficiency of the TiO_2 photocatalyst is strongly related to the crystalline form and crystallization degree, the particle size, the pore structure and the surface chemistry, etc. Therefore, the preparation method must play a key role in determining its activity. Usually, the treatment of the precursor by direct drying and calcination may cause the agglomeration of the small particles and the collapse of pore structure. Recently, the treatment of the catalyst precursor under supercritical conditions becomes more and more attractive since the resulting catalyst could remain in the pore structure as that in the gel [14–17]. In this paper, we report a novel SO_4^{2-}-doped TiO_2 photocatalyst (SO_4^{2-}/TiO_2) prepared by treating the xerogel under supercritical conditions. During liquid-phase photocatalytic degradation of phenol, this catalyst exhibited higher activity and longer lifetime than the corresponding undoped TiO_2 and SO_4^{2-}/TiO_2 obtained via direct drying [18,19], obviously showing the superiority of the supercritical drying and the promoting effect of the SO_4^{2-}-dopant.

* Corresponding author. Tel.: +86 21 64322141; fax: +86 21 64322142.
E-mail address: hexing-li@shtu.edu.cn (H. Li).

1381-1169/$ – see front matter © 2004 Elsevier B.V. All rights reserved.
doi:10.1016/j.molcata.2004.09.028

2. Experimental

2.1. Catalyst preparation

At 313 K, 10 ml of Ti(On-C_4H_9)$_4$ was added slowly into 40 ml of alcohol (100%) to form solution A. Meanwhile, 2.5 ml of dilute HNO_3 solution (1:5, v/v) was mixed with 10 ml alcohol to prepare solution B. Then, the solution B was added dropwise into the solution A within ~20 min under vigorous stirring. The solution was kept stirred continuously for 1 h until the formation of the TiO_2 gel. After being aged for 48 h at 318 K, the as-prepared TiO_2 xerogel was dried under supercritical conditions described as follows. At room temperature, a 500 ml autoclave containing the as-prepared TiO_2 xerogel and 250 ml of alcohol was swept by pure N_2 for 1 h to remove the O_2 inside. Then, the autoclave was heated at the speed of 4 K/min up to 533 K, at which the pressure reached 11.5 MPa. The system was kept at that temperature and pressure for 2 h and then the alcohol vapor was removed slowly. Once the pressure decreased down to the normal pressure, the N_2 flow was passed through autoclave for about 3–5 min. After being cooled down to room temperature in the N_2 flow, the TiO_2 xerogel was calcined at a given temperature for 10 h to remove the residual organic compounds and the solvent alcohol. The optimum calcination temperature was found to be 673 K. Finally, the as-prepared TiO_2 sample was crushed and kept in vacuum until the time of use. When the H_2SO_4 dilute solution was used instead of HNO_3, the SO_4^{2-}/TiO_2 sample was obtained since different from NO_3^-, SO_4^{2-} could not be removed during the calcination. Adjusting the volume of H_2SO_4 solution (1.0, 1.5, 2.0, 2.5 and 3.0 ml) resulted in different sulfur content in the SO_4^{2-}/TiO_2 sample, which was expressed in $\chi_{S/Ti}$, the molar ratio between S and Ti. In this way, $\chi_{S/Ti} = 0$ refers to undoped TiO_2. All these samples were denoted as TiO_2(SC) and SO_4^{2-}/TiO_2(SC), respectively, where SC refers to supercritical conditions. For comparison, both the TiO_2 and the SO_4^{2-}/TiO_2 samples were also prepared by direct drying and calcining the precursors, which were denoted as TiO_2(DC) and SO_4^{2-}/TiO_2(DC), respectively.

2.2. Catalyst characterization

The structure of the undoped and the SO_4^{2-}-doped TiO_2 samples was confirmed by both X-ray diffraction (XRD, Rigacu Dmax-3C with Cu Kα radiation) and FT-IR (NEXUS 470). The surface morphology and the particle size were observed through the transmission electronic micrograph (TEM, JEM-2010). FTIR-pyridine thermodesorption was employed to determine both the number and the type of the acidic sites on the surface of the as-prepared catalysts. Since the experiments were carried out in the vacuum condition, the conversion from Lewis acidic sites to Brønsted acidic sites induced by the adsorption of water on the Lewis acidic sites could be excluded [20]. The surface electronic states were determined by the X-ray photoelectron spectroscopy (XPS, Perkin-Elmer PHI 5000C). All binding energy (BE) values were calibrated by using the standard BE value of contamination carbon (C 1s = 284.6 eV) as a reference. The UV light absorption and excitation were investigated by photoluminescence spectra (PLS, Varian Cary-Eclipse 500).

2.3. Activity test

The liquid-phase photocatalytic degradation of phenol was carried out at 303 K in a self-designed 200 ml reactor containing 0.05 g catalyst, and 30 ml of phenol aqueous solution (0.1 g/l). The mixture was stirred for 1 h until the adsorption equilibrium was reached. Then, the photocatalysis was started by irradiating the reaction mixture with UV light at 4 cm above the solution. Three 8 W lamps with characteristic wavelengths of 254, 310 and 365 nm, respectively, were used as a mixed UV light source. In order to ascertain the role of mass transfer, the catalyst amount was varied from 0.02 to 0.10 g and the speed of agitation was varied from 800 to 1200 rpm. In view of the observation that the reaction rate was independent of the stirring rate and that it varied linearly with the catalyst amount, it could be concluded that the stirring rate of 1000 rpm was high enough so that the phenol degradation rates were independent of mass transfer. After reaction for 3 h, the catalyst was separated from the solution and the phenol left in the solution was analyzed by a UV spectrophotometer (UV 7504/PC) at $\lambda = 270$ nm, the characteristic wavelength of phenol. A preliminary test showed that there was a good linear relationship between the absorbance and the phenol concentration. According to the reference experiments, the phenol degradation after 3 h was less than 5% in the absence of either the catalyst or the UV light and thus could be neglected in comparison with that in the presence of both the catalyst and the UV source. The reproducibility of the results was checked by repeating the runs at least three times and was found to be within acceptable limits (±5%).

3. Results and discussion

Fig. 1 shows the XRD patterns of both TiO_2(SC) and TiO_2(DC) after being calcined at elevated temperatures. Unlike the commercially available TiO_2(P-25) [21] which displayed both the anatase phase (~75%) and the rutile phase (~25%) corresponding to $2\theta = 29.5^\circ$ and 32.0°, respectively, the TiO_2(SC) sample exhibited the well-crystallized anatase phase. The crystallization degree increased slightly with the increase in calcination temperature from 573 to 973 K. No significant rutile phase appeared even at 973 K, showing the excellent thermal stability of TiO_2(SC). In contrast, TiO_2(DC) exhibited very low crystallization degree of anatase. Treatment at 973 K resulted in a structural transformation from anatase to rutile phase due to the poor thermal stability. From Fig. 2, one can see that modification of TiO_2 sample with the SO_4^{2-}-dopant under supercritical conditions did not generate any new phases, but the intensity of the XRD

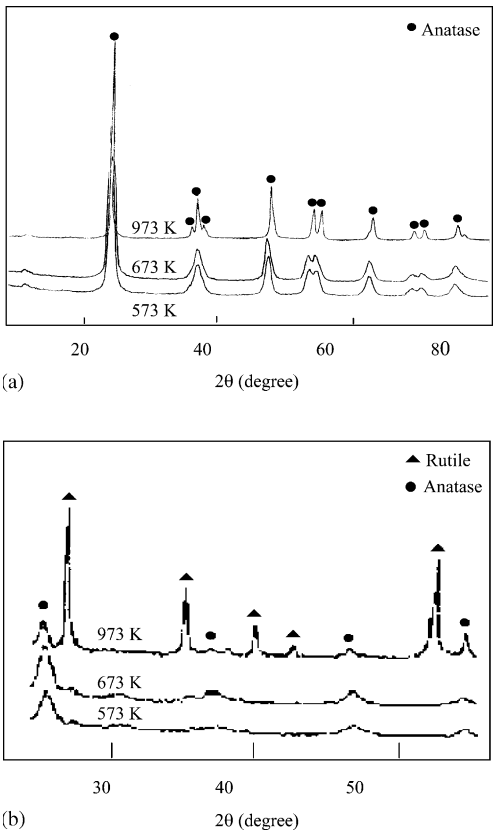

Fig. 1. XRD patterns (a) TiO_2(SC) and (b) TiO_2(DC) treated at different temperatures.

peaks increased gradually with the increase in $\chi_{S/Ti}$, showing that the SO_4^{2-}-modification was favorable for the crystallization of anatase phase [22].

As shown in Fig. 3, the TEM morphologies revealed that both TiO_2(SC) and TiO_2(DC) samples were present in the spherical nanoparticles with similar particle size around 10–20 nm but the nanoparticles in TiO_2(SC) are distributed more homogeneously. Modification with SO_4^{2-} further improved the particle distribution. From the isothermal curves

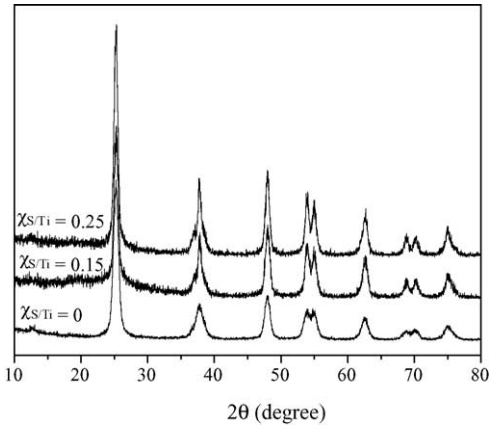

Fig. 2. XRD patterns of SO_4^{2-}/TiO_2(SC) samples with different $\chi_{S/Ti}$, where $\chi_{S/Ti} = 0$ refers to the undoped TiO_2 sample.

of nitrogen adsorption and desorption at 77 K, the surface area (S_{BET}), pore volume (V_P) and average pore diameter (d_P) were calculated by using the BJH method. As shown in Table 1, TiO_2(SC) exhibited much higher surface area than TiO_2(DC). Since the TEM morphologies demonstrated that both the samples exhibited similar particle sizes, one could conclude that the higher surface area of TiO_2(SC) was mainly attributed to its larger pore volume and pore size. This could be easily understood by considering the unique role of the supercritical conditions since removal of the solvent under such conditions might maintain the pore structure in the gel owing to the lack of surface tension effect [14–17]. On the other hand, severe collapse of the pore structure would occur when the solvent in the gel was removed by direct drying, resulting in an abrupt decrease in the pore volume and pore size and thus, the surface area. For SO_4^{2-}/TiO_2(SC), both d_P and V_P increased monotonously with the increase in $\chi_{S/Ti}$, possibly owing to the coordination between SO_4^{2-} and TiO_2 in the network. This was confirmed by the FTIR spectrum. As shown in Fig. 4, both the samples exhibited strong absorption at 1630 and 3410 cm^{-1}, corresponding to the stretching vibration of the hydroxyl group on the surface [23]. The SO_4^{2-}/TiO_2(DC) sample exhibited two peaks around 937 and 980 cm^{-1}, indicative of the surface adsorbed SO_4^{2-} species [24]. However, no absorbance bands in the range from 900 to 990 cm^{-1} were observed in SO_4^{2-}/TiO_2(SC), suggesting that nearly all the SO_4^{2-} species entered the network of TiO_2. The absorbance bands at 1040 and 1140 cm^{-1} demonstrated that the SO_4^{2-}-dopant might coordinate with TiO_2 in the network in the following mixed models [24].

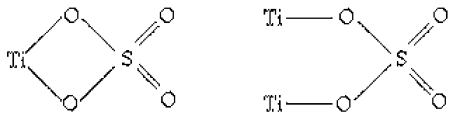

Coordination models between SO_4^{2-} and TiO_2

According to the FTIR-pyridine thermodesorption spectra (Fig. 5), SO_4^{2-}/TiO_2(DC) displayed both the Lewis acidic sites corresponding to absorbance bands at 1444, 1493, 1576 and 1603 cm^{-1} and the Brønsted acidic sites corresponding to a broad absorbance band around 1539 cm^{-1} [18]. The Brønsted acidic sites may result from the surface SO_4^{2-} species adsorbed by TiO_2 while the Lewis acidic sites could be attributed to the coordination between SO_4^{2-} and TiO_2 in the network. As shown in the above coordination models,

Table 1
Structural parameters of the as-prepared TiO_2 and SO_4^{2-}/TiO_2 samples

Samples	$\chi_{S/Ti}$	d_P (nm)	V_P (ml/g)	S_{BET} (m^2/g)	Degradation (%)
TiO_2(P-25)	0	20	0.25	45	67
TiO_2(DC)	0	5.4	0.037	27	39
TiO_2(SC)	0	20	0.449	81	61
SO_4^{2-}/TiO_2(SC)	0.15	29	0.518	105	89
SO_4^{2-}/TiO_2(SC)	0.25	37	0.761	100	68

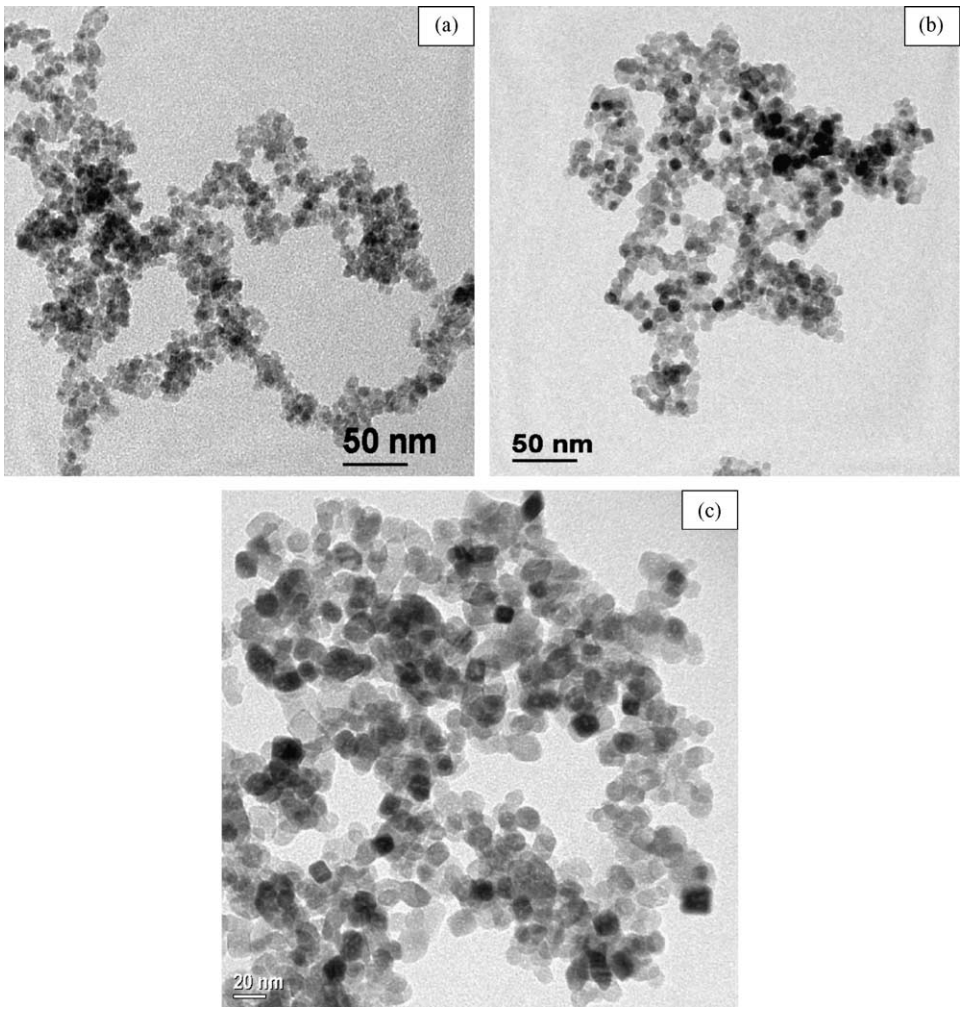

Fig. 3. TEM morphologies of (a) TiO_2(DC), (b) TiO_2(SC) and (c) SO_4^{2-}/TiO_2(SC) with $\chi_{S/Ti} = 0.15$.

the existence of S=O covalent bonds in the TiO_2 network were the important source for generating the Lewis acidic sites [24,25]. Unlike SO_4^{2-}/TiO_2(DC), SO_4^{2-}/TiO_2(SC) displayed only the Lewis acidic sites, which was consistent with the aforementioned conclusion that nearly all the SO_4^{2-} species were present in the TiO_2 network. Besides, SO_4^{2-}/TiO_2(SC) exhibited much stronger peak intensity than SO_4^{2-}/TiO_2(DC), implying that there were more Lewis acidic sites in SO_4^{2-}/TiO_2(SC).

Fig. 6 shows the XPS spectra of both the TiO_2 and SO_4^{2-}/TiO_2 samples obtained under supercritical conditions. It was found that the modification of TiO_2 with the SO_4^{2-}-dopant had no significant influence on the position of the peak in the Ti_{2p} level. However, the addition of the SO_4^{2-}-dopant resulted in the positive shift of the binding energy of oxygen by 0.5 eV. Meanwhile, the binding energy of the sulfur shifted negatively by 0.5 eV in comparison with the standard binding energy of the sulfur in pure SO_4^{2-}. These results demonstrated that electrons partially transferred from oxygen to sulfur in SO_4^{2-}/TiO_2(SC). Although the electronegativity of oxygen is slightly higher than that of sulfur, the larger size of sulfur atom than that of oxygen atom may account for the electron transfer from oxygen to sulfur atom.

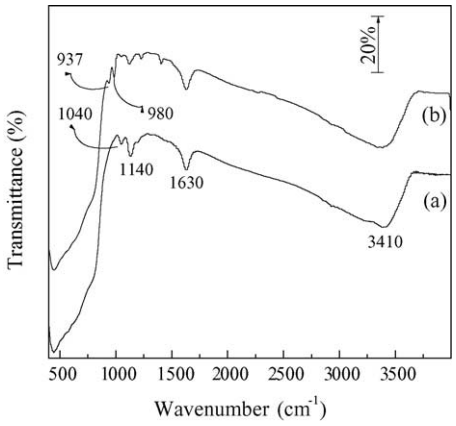

Fig. 4. FTIR spectra of (a) SO_4^{2-}/TiO_2(SC) with $\chi_{S/Ti} = 0.15$ and (b) SO_4^{2-}/TiO_2(DC) with $\chi_{S/Ti} = 0.20$.

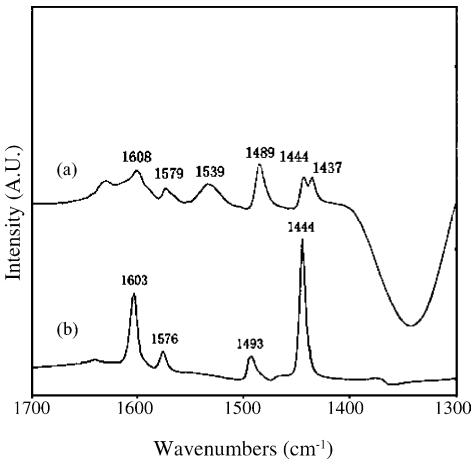

Fig. 5. FTIR-pyridine thermodesorption spectra at room temperature of (a) SO_4^{2-}/TiO_2(DC) with $\chi_{S/Ti} = 0.20$ and (b) SO_4^{2-}/TiO_2(SC) with $\chi_{S/Ti} = 0.15$.

The photoluminescence spectra (PLS) demonstrated that both TiO_2(SC) and TiO_2(DC) samples exhibited two PLS peaks, as shown in Fig. 7. The signals at about 382 nm could be attributed to an emission peak from band edge free excitation, mainly corresponding to the oxygen vacancies and/or defects of the TiO_2 particles [26]. The stronger emission peak at 382 nm implied the presence of more oxygen vacancies and/or defects. Up to now, still there is no clear relationship between the photoluminescence intensity at about 560 nm and the absorption coefficient, especially in the case of the powdered system. Liu et al. [27] suggested that the signal at about 560 nm was possibly related to the ability of TiO_2 sample for absorbing UV light and that the weaker photoluminescence intensity demonstrated that TiO_2(SC) may absorb more UV lights. To support the above conclusion, UV–vis spectra of both SO_4^{2-}/TiO_2(SC) and SO_4^{2-}/TiO_2(DC) were measured. As shown in Fig. 8, the SO_4^{2-}/TiO_2(SC) sample displayed higher absorption coefficient in the UV region than the corresponding SO_4^{2-}/TiO_2(DC) sample.

Fig. 9 shows the dependence of phenol conversion on the $\chi_{S/Ti}$ of SO_4^{2-}/TiO_2 catalysts obtained via supercritical drying and direct drying, respectively. One can see that the phenol conversion increased gradually with $\chi_{S/Ti}$ regardless of the preparation methods. The highest activity of SO_4^{2-}/TiO_2(SC) was obtained at $\chi_{S/Ti} = 0.15$, which was much higher than that of the commercially available TiO_2 catalyst (P-25), as shown in Table 1. The promoting effect of the SO_4^{2-}-dopant on the activity could be understood by considering the following factors: (1) The SO_4^{2-}-modification resulted in the higher surface area and larger pore size as well as pore volume (see Table 1), which allowed more phenol molecules to be adsorbed on the catalyst surface, facilitating the phenol degradation. (2) The SO_4^{2-}-modification enhanced the crystallization degree of the anatase phase (see Fig. 2), which has been claimed to be favorable for the phenol degradation [28]. (3) The SO_4^{2-}-modification generated more acidic sites on the TiO_2 surface. These acidic sites were

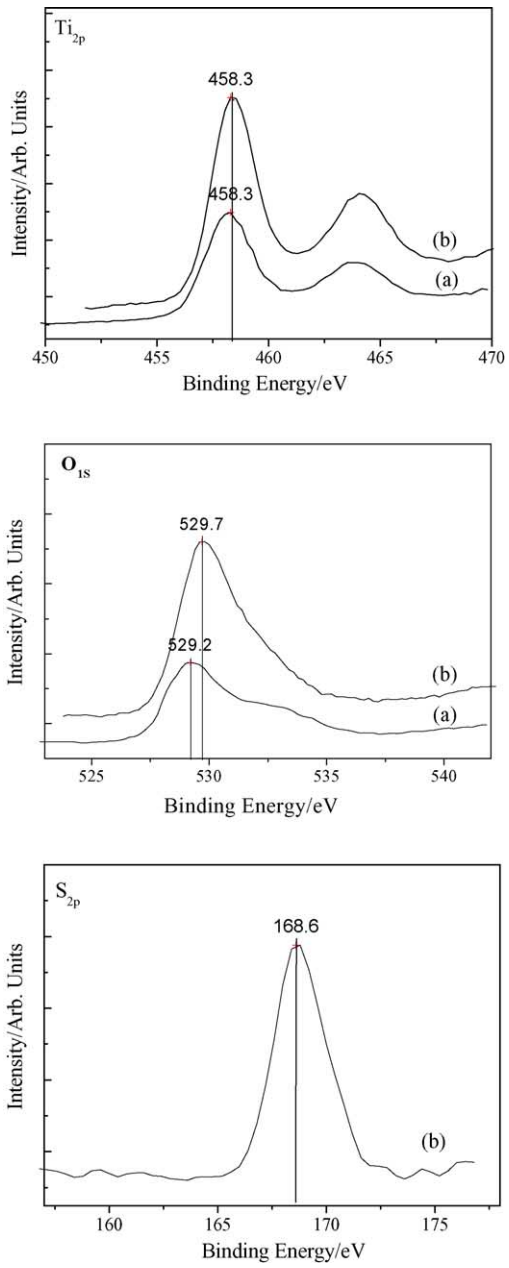

Fig. 6. XPS spectra of (a) undoped TiO_2(SC) and (b) SO_4^{2-}/TiO_2(SC) with $\chi_{S/Ti} = 0.15$.

beneficial for the adsorption of phenol molecules and for the inhibition of the recombination between photo-induced electrons and holes, since photo-induced electrons could be captured by these acidic sites [29]. Thus, the quantum efficiency of the TiO_2 photocatalyst was improved, resulting in the higher photocatalytic activity. (4) As discussed above based on Fig. 6, the SO_4^{2-}-modification resulted in the electron-deficient oxygen which could also serve as an electron trap to inhibit the recombination between photo-induced electrons and holes and thus, promoted the oxidative degradation of phenol. However, very large amount of the SO_4^{2-}-dopant was harmful for the activity possibly due to the coverage of

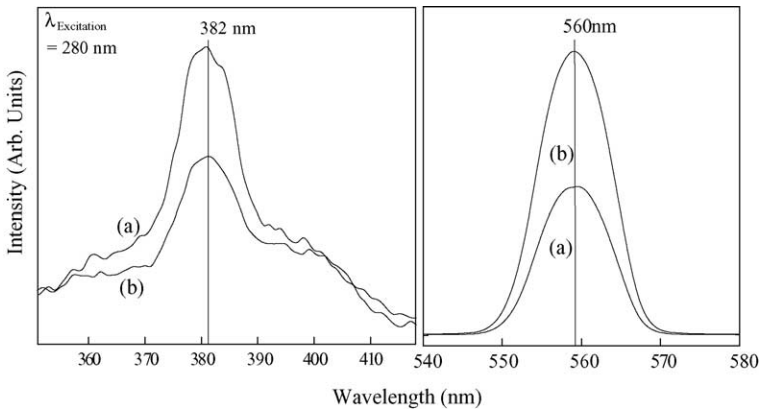

Fig. 7. Photoluminescent spectra (PLS) of (a) TiO_2(SC) and (b) TiO_2(DC).

too many TiO_2 active sites by the SO_4^{2-}-additives. The optimum $\chi_{S/Ti}$ values for SO_4^{2-}/TiO_2(SC) and SO_4^{2-}/TiO_2(DC) were found to be 0.15 and 0.20, respectively.

Concerning the TiO_2 samples obtained under different conditions, TiO_2(SC) exhibited much higher activity than TiO_2(DC), showing the superiority of the supercritical drying over the direct drying. This could be attributed to the higher surface area, larger pore size and pore volume [30] as well as the higher crystallization degree of the anatase phase, as shown in Table 1 and Fig. 1. Besides, from Fig. 7 one can see that TiO_2(SC) displayed more oxygen vacancies and/or defects which could capture the photo-induced electrons and thus could effectively inhibit the recombination of the photo-induced electrons and holes. Meanwhile, Fig. 8 shows that TiO_2(SC) may absorb more UV light which might generate more charge carriers served as active sites for phenol degradation. This excellent UV light absorption property was also responsible for the higher activity of TiO_2(SC) than TiO_2(DC), since the quantum efficiency was enhanced.

Considering the SO_4^{2-}-modification under different conditions, one can see that the phenol conversion over SO_4^{2-}/TiO_2(SC) increased more rapidly with $\chi_{S/Ti}$ than that over SO_4^{2-}/TiO_2(DC), possibly due to the different states of the SO_4^{2-}-dopant in two catalysts. As shown in Fig. 5, some SO_4^{2-} species in SO_4^{2-}/TiO_2(DC) were adsorbed on the TiO_2 surface producing Brønsted acidic sites while the others were coordinated with TiO_2 in network corresponding to Lewis acidic sites. Unlike the SO_4^{2-} species in SO_4^{2-}/TiO_2(DC), nearly all the SO_4^{2-} species in SO_4^{2-}/TiO_2(SC) were coordinated with TiO_2 in the network producing only Lewis acidic sites. It was claimed that the Lewis acidic sites had stronger affinity for the electrons than the Brønsted acidic sites [31]. The more Lewis acidic sites in SO_4^{2-}/TiO_2(SC) could capture more photo-induced electrons which could effectively protect the photo-induced holes (the active sites for phenol oxidation) from recombination with electrons. This could enhance the

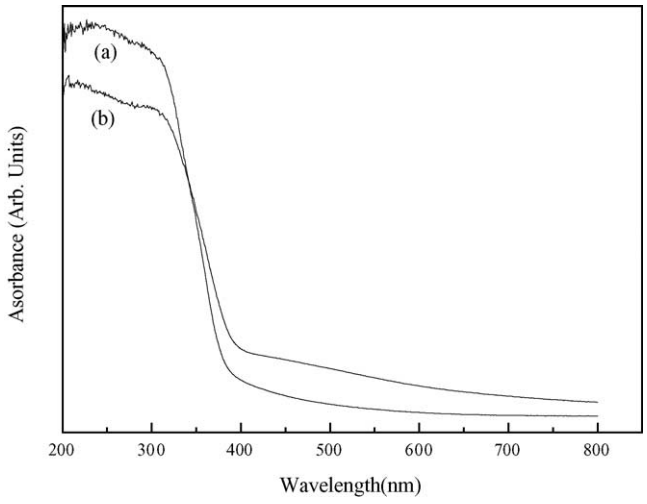

Fig. 8. UV–vis spectra of (a) SO_4^{2-}/TiO_2(SC) with $\chi_{S/Ti}$ = 0.15 and (b) SO_4^{2-}/TiO_2(DC) with $\chi_{S/Ti}$ = 0.20.

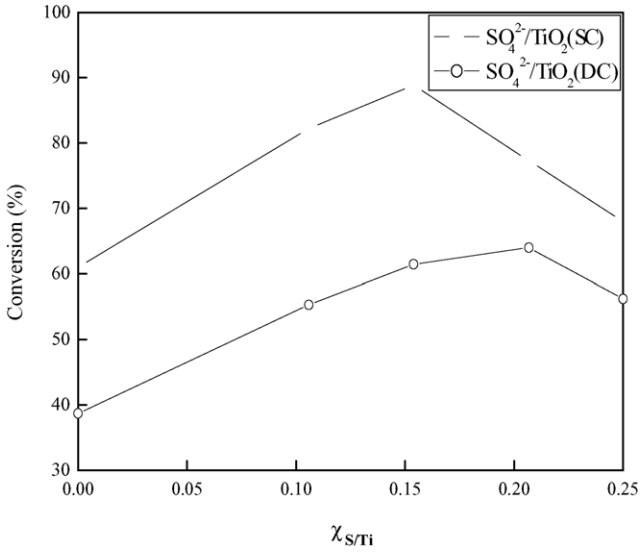

Fig. 9. Dependence of phenol conversion on the $\chi_{S/Ti}$ of (a) the SO_4^{2-}/TiO_2(SC) and (b) the SO_4^{2-}/TiO_2(DC). Reaction conditions: 0.050 g catalyst, 30 ml phenol aqueous solution (0.1 g/l), three 8 W lamps with characteristic wavelengths of 254, 310 and 365 nm as UV light source mounted at 4 cm above the solution, T = 303 K, stirring rate = 1000 rpm, and reaction time = 3 h.

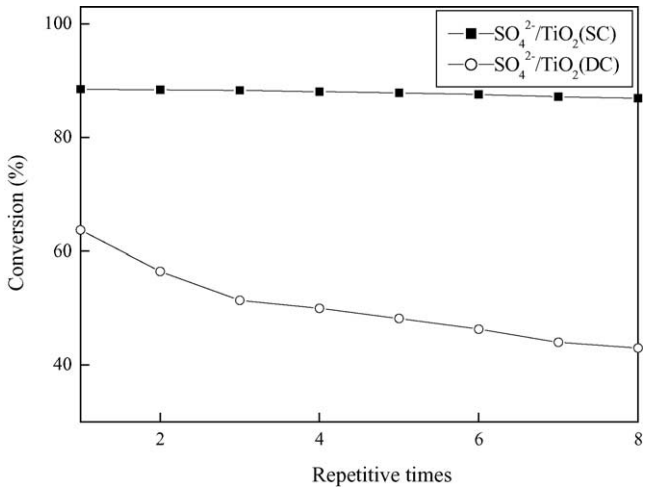

Fig. 10. Durability test of (a) the SO_4^{2-}/TiO_2(SC) with $\chi_{S/Ti} = 0.15$ and (b) SO_4^{2-}/TiO_2(DC) with $\chi_{S/Ti} = 0.20$. Reaction conditions are given in Fig. 8. Each run of repetitive experiments lasted for 3 h.

quantum efficiency, accounting for the higher activity of SO_4^{2-}/TiO_2(SC) than that of SO_4^{2-}/TiO_2(DC). Meanwhile, the SO_4^{2-}-modification under supercritical conditions also resulted in more electron-deficient oxygen. These oxygen species may serve as the trap for photo-induced electrons and thus, enhanced the quantum yield of the photocatalysis, since the recombination between photo-induced electrons and holes was effectively inhibited.

Besides the higher activity, SO_4^{2-}/TiO_2(SC) also exhibited much longer lifetime than SO_4^{2-}/TiO_2(DC). As shown in Fig. 10, SO_4^{2-}/TiO_2(SC) with $\chi_{S/Ti} = 0.15$ could be used repetitively for more than eight times (each for 3 h) without significant decrease in activity. In contrast, the activity of SO_4^{2-}/TiO_2(DC) with $\chi_{S/Ti} = 0.20$ was considerably decreased even when it was used for the second time. The greater durability of SO_4^{2-}/TiO_2(SC) could also be attributed to the coordination between SO_4^{2-} and TiO_2 in the network. Such coordinating bond was very strong which could prevent the leaching of the SO_4^{2-}-dopant from SO_4^{2-}/TiO_2 catalyst during photocatalysis. This was further confirmed by product analysis which revealed that no significant amount of sulfur species were detected in the solution even after SO_4^{2-}/TiO_2(SC) being used repetitively for eight times while great portion of sulfur species were detected in the solution when SO_4^{2-}/TiO_2(DC) was employed. After being used repetitively for eight times, the activity of SO_4^{2-}/TiO_2(DC) decreased down to that of the undoped TiO_2(DC), indicating that nearly all the SO_4^{2-}-dopants have been leached out from the catalyst.

4. Conclusions

This study reported a new SO_4^{2-}/TiO_2(SC) photocatalyst obtained by drying the catalyst precursor under supercritical conditions for liquid-phase phenol degradation and supplied a powerful way to enhance the activity and the durability of the TiO_2 photocatalyst. More specially, the following points are highlighted:

1. Treatment of the catalyst precursor obtained from the sol–gel method under supercritical conditions might produce the undoped and the SO_4^{2-}-doped TiO_2 catalysts with the well-crystallized anatase phase, higher surface area, larger pore size and pore volume as well as more oxygen vacancies and/or defects, which were favorable for the photocatalytic degradation of phenol.
2. Modification with the SO_4^{2-}-dopant could enhance the activity of TiO_2 owing to the increase in the crystallization degree of anatase, the surface area, the pore size, the pore volume, and especially the surface acidity.
3. SO_4^{2-}-modification through supercritical drying was more powerful than that via direct drying, since nearly all the SO_4^{2-} species could coordinate with TiO_2 in the network which could generate more Lewis acidic sites for capturing photo-induced electrons and thus enhanced the quantum yield of the photocatalysis, since the recombination between the photo-induced electrons and holes was effectively inhibited. This could also account for the longer lifetime of the SO_4^{2-}/TiO_2(SC) than of the SO_4^{2-}/TiO_2(DC), since the leaching of SO_4^{2-} species in the SO_4^{2-}/TiO_2(SC) was more difficult owing to the stronger coordination bond.

Acknowledgments

This work was supported by the National Natural Science Foundation of China (20377031) and the Natural Science Foundation of Shanghai Science and Technology Committee (02DJ14005, 03DJ14005).

References

[1] M.R. Hoffmann, S.T. Martin, W. Choi, D.W. Bahnemann, Chem. Rev. 95 (1995) 69.
[2] J.M. Herrmann, C. Guillard, P. Pichat, Catal. Today 17 (1993) 7.
[3] H. Yamashita, Y. Ichihashi, M. Anpo, M. Hashimoto, C. Louis, M. Che, J. Phys. Chem. 100 (1996) 16041.
[4] H. Yamashita, Y. Ichihashi, M. Harada, J. Catal. 158 (1996) 97.
[5] M.A. Fox, M.T. Dulay, Chem. Rev. 93 (1993) 341.
[6] A.L. Linsebigler, G. Lu, J.T. Yates Jr., Chem. Rev. 95 (1995) 735.
[7] J.C. Yu, J.G. Yu, W.K. Ho, Z.T. Jiang, L.Z. Zhang, Chem. Mater. 14 (2002) 3808.
[8] C. Kormann, D.W. Bahnemann, M.R. Hoffmann, J. Phys. Chem. 92 (1988) 5196.
[9] S. Klosek, D. Raftery, J. Phys. Chem. 105 (2001) 2815.
[10] S. Al-Qaradawi, S.R. Salman, J. Photochem. Photobiol. A: Chem. 148 (2002) 161.
[11] D.B. Haddow, S. Kothari, P.F. James, R.D. Short, P.V. Hatton, R. van Noort, Biomaterials 17 (1996) 502.
[12] S. Peres-Durand, J. Rouviere, C. Guizard, Colloids Surf. A: Physicochem. Eng. Asp. 98 (1995) 252.

[13] E. Piera, J.A. Ayllon, X. Domenech, J. Peral, Catal. Today 76 (2002) 259.
[14] V. Gourinchas-Courtecuisse, J.F. Bocquet, K. Chhor, C. Pommier, J. Supercrit. Fluids 9 (1996) 222.
[15] J.F. Bocquet, K. Chhor, C. Pommier, Mater. Chem. Phys. 57 (1999) 274.
[16] J. Brasseur-Tilmant, K. Chhor, P. Jestin, C. Pommier, Mater. Res. Bull. 34 (1999) 2013.
[17] R. van Grieken, G. Calleja, G.D. Stucky, J.A. Melero, A. Garcia, J. Iglesia, Langmuir 19 (2003) 3973.
[18] G. Colón, M.C. Hidalgo, J.A. Nav'yo, Appl. Catal. B: Environ. 45 (2003) 39.
[19] D.S. Muggli, L. Ding, Appl. Catal. B: Environ. 32 (2001) 181.
[20] K. Tanabe, in: J.R. Anderson, M. Boudart (Eds.), Catal. Sci. Technol., 2, 1981, 231.
[21] Z. Ding, G.Q. Lu, P.F. Greenfield, J. Phys. Chem. 104 (2000) 4815.
[22] S. Yamazaki, N. Fujinaga, K. Araki, Appl. Catal. A: General 210 (2001) 97.
[23] W.S. Li, Z.Q. Shen, Y.F. Zhang, Eur. Poly. J. 37 (2001) 1185.
[24] T. Jin, M. Machida, T. Yamaguchi, K. Tanabe, Inorg. Chem. 23 (1984) 4396.
[25] L.D. Zhang, C.M. Mou, Nanostruct. Mater. 6 (1995) 831.
[26] H. Yamashita, Y. Ichihashi, M. Anpo, J. Phys. Chem. 100 (1996) 16041.
[27] H. Liu, H.J. Wu, F.X. Sun, Y.L. Yao, M. Wu, W.Z. Li, Chinese J. Mol. Catal. 15 (2001) 47.
[28] S. Yamazaki, N. Fujinaga, K. Araki, Appl. Catal. A: General 210 (2003) 97.
[29] R.A. Young, P. Desai, Arch. Nauki. Mater. 10 (1989) 71.
[30] S. Yin, T. Sato, Ind. Eng. Chem. Res. 39 (2000) 4530.
[31] G.A. Mekhemer, A.K. Nohman, N.E. Fouad, Coll. Surf. 161 (2000) 439.